An Experimentally Validated Technique for the Real-Time Management of Wrist Singularities in Nonredundant Anthropomorphic Manipulators

Corrado Guarino Lo Bianco, *Senior Member, IEEE*, and Marina Raineri

***Abstract*— The automatic management of kinematic singularities that are typical for trajectories planned in the operational space is arousing a renewed interest among the scientific community because the most recent strategies make it possible their real-time management. The approach described in this paper allows executing trajectories in the operational space which pass through wrist singularities. It introduces several novelties with respect to known alternative strategies. First, it is conceived for trajectories which are planned on-the-fly. Second, singularities are avoided by changing slightly the tool frame orientation while strictly preserving both the assigned Cartesian path and time law. Finally, the approach is effective also for manipulators moving at standard operative speeds, and it explicitly handles given limits on joint velocities and accelerations. In this paper, an approach proposed in early works is revised in order to make it ready for an industrial implementation. In particular, a procedural method is proposed for the tuning of the algorithm so as to make it more deterministic and to increase the success rates. Furthermore, the singularity avoidance problem is theoretically analyzed in order to devise a necessary condition for the existence of a solution. Results are experimentally validated through an anthropomorphic industrial manipulator.**

***Index Terms*— Motion control, nonredundant manipulators, real-time systems, robot motion, singularity avoidance.**

NOMENCLATURE

The notation used along the paper is summarized in the following. Missing terms are directly defined in the text.

$s \in \mathbb{R}^+$	Curvilinear coordinate which identifies the position along the path.
$\mathbf{q} \in \mathbb{R}^6$	Vector of the joint variables.
${}^0_T\mathbf{R} \in \mathbb{R}^{3\times3}$	Rotation matrix associated with the tool-frame orientation.
$\mathbf{p}_T \in \mathbb{R}^3$	Position of the tool frame.
$\boldsymbol{\omega}_T \in \mathbb{R}^3$	Angular velocity of the tool frame.
$\mathbf{v}_T \in \mathbb{R}^3$	Linear velocity of the tool frame.
$\boldsymbol{\alpha}_T \in \mathbb{R}^3$	Angular acceleration of the tool frame.
$\mathbf{a}_T \in \mathbb{R}^3$	Linear acceleration of the tool frame.
$\mathbf{J}_T(\mathbf{q}) \in \mathbb{R}^{6\times6}$	Jacobian matrix associated with the tool frame.

Manuscript received September 14, 2018; revised January 11, 2019; accepted April 17, 2019. Date of publication June 3, 2019; date of current version June 11, 2020. Manuscript received in final form April 18, 2019. Recommended by Associate Editor G. Hu. *(Corresponding author: Corrado Guarino Lo Bianco.)*

The authors are with the Department of Engineering and Architecture, University of Parma, 43121 Parma, Italy (e-mail: corrado.guarinolobianco@unipr.it; marina.raineri@unipr.it).

Color versions of one or more of the figures in this brief paper are available online at http://ieeexplore.ieee.org.

Digital Object Identifier 10.1109/TCST.2019.2912787

T indicates the tool frame. According to the definitions, $\mathbf{p}_T(s)$ and ${}^0_T\mathbf{R}(s)$ specify the position and the orientation of the tool frame expressed as functions of the curvilinear coordinate. Trajectories are obtained by combining positions and orientations with time-law $s(t)$, so that $\mathbf{p}(t) := \mathbf{p}[s(t)]$ is a Cartesian trajectory, whereas ${}^0_T\mathbf{R}(t) := {}^0_T\mathbf{R}[s(t)]$ is an orientation trajectory. The same notation is used for velocities and accelerations of the tool frame.

I. INTRODUCTION

ONE of the major problems that must be tackled when trajectories are planned in the operational space is associated with the management of the so-called kinematic singularities, i.e., configurations in which bounded Cartesian speeds lead to endless joint speeds and bounded joint torques lead to unbounded end-effector forces. Anthropomorphic manipulators admit three types of singularities: 1) shoulder singularities are only significant for hanging robots and appear when the wrist crosses the first axis; 2) elbow singularities are scarcely relevant since they occur at the border of the workspace, i.e., in areas which are seldom used; and 3) wrist singularities appear when the fourth and the sixth joint axes are aligned. This paper focuses on the management of wrist singularities since they may occur in any point of the workspace and, consequently, they are relevant in many practical applications.

Kinematic singularities can be handled in several ways. The most commonly used approaches react to singularities by marginally modifying the assigned paths and time laws. Planners for the operational space are typically based on the functional scheme in Fig. 1: the Cartesian trajectory planner is immediately followed by an inverse kinematics block, which is also in charge for the management of possible kinematic singularities. All works proposed during 80th and 90th were practically based on such conceptual scheme.

Many of the techniques in the literature derive from the original approach proposed in [1] for the solution of the inverse kinematics of redundant manipulators: the generated joint reference signals guarantee that the trajectory in the operational space is exactly executed, while available degrees of freedom are used to accomplish secondary tasks. The strategy was later revised and better formalized in [2]. For the first time, it was explicitly remarked that such technique is potentially suited for the management of kinematic singularities. The methodology was later extended in [3] and [4] in order to manage the constraints through a task priority approach. The task priority

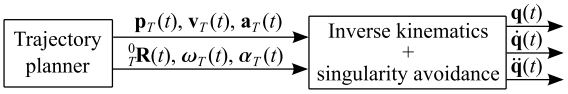

Fig. 1. Typical planner scheme for trajectories in the operational space.

strategy was later revised in [5] by explicitly considering its use for the management of kinematic singularities.

In the same years, other alternative methods were proposed for the solution of the inverse kinematic problem. Some of them were based on a damped least-square approach [6], [7], while others were based on closed-loop schemes and were able to manage constrained problems by means of a proper augmentation of the task space dimension [8], [9].

Research studies based on the above methods are prosecuted up until now as proved by several works in the literature [10]–[13]. All mentioned techniques, when extended to nonredundant manipulators, show some common characteristics:

1) singularities are managed by introducing small position and orientations errors;
2) the amplitude of such errors is kept small through proper tunings, but explicit bounds are not imposed; and
3) velocities and accelerations are generically limited, but they are not forced within given bounds.

Such characteristics may or may not be appropriate depending on the application at hand. For example, there exist applications that do not allow deviations from the assigned Cartesian path, so that the problem must be tackled through alternative methods. If the path does not exactly cross singular configurations and the time law is not assigned, control methods based on predictive controllers can be used for the generation of efficient trajectories [14]–[18]. Alternatively, if the time law is assigned, the trajectory can be slowed down so as to preserve both path and orientation of the end-effector [19]–[21].

The situation becomes more critical if the assigned path crosses a kinematic singularity and the time law is given and unmodifiable. In that case, singular points can be managed by slightly modifying the nominal orientation of the end-effector. In many industrial processes, indeed, small orientation changes have a minimal impact on the product quality, while speed and/or path changes may worsen the final result. This is the case, for example, of welding, gluing, or painting processes [22]–[24]. The acquired degrees of freedom can be used to avoid the singular configurations by preserving, simultaneously, both the assigned Cartesian path and the time law. The Singularity Avoidance System (SAS), i.e., the algorithm considered in this paper, belongs to this class of methods.

The mentioned problem may be alternatively handled by means of offline planners, but nowadays, applications require trajectories generated on-the-fly on the basis of the data acquired by perceptual sensors. Some real-time planners, able to preserve the Cartesian path, have been already proposed. They are typically conceived for the generation of slow motions like the ones deriving, for example, from the use of teaching devices handled by human operators [25]–[27]. Conversely, the SAS manages wrist singularities of nonredundant anthropomorphic manipulators through a real-time strategy whose evaluation times are in the order of a few microseconds. The SAS has characteristics which are not owned by the methods previously cited. In particular, if a singularity is encountered the Cartesian path and the time law are preserved with certainty, while the tool-frame orientation is slightly modified with respect to the nominal reference. The orientation change is superiorly bounded. Furthermore, joint velocities and accelerations are not generically kept small, but they are explicitly constrained within assigned limits. Finally, the SAS is conceived to work at normal operative speeds, i.e., its usability is not limited to slow motions.

The first SAS release appeared in [28] for the management of trajectories passing close to wrist singularities, while a subsequent version, proposed in [29], allowed improved performances with the aid of nonlinear optimization techniques. The scheme recently proposed in [30]—differently from the solutions appeared in [28], in [29], or in any other paper in the literature—can even manage trajectories which cross singularities, with computational times which are compatible with the ones required by real-time applications.

In this paper, the SAS implementation proposed in [30] is revised to achieve better performances. More precisely, the tuning procedure of the algorithm has been totally reconsidered so as to make the SAS "industrially ready": the new release handles wrist singularities of the whole workspace with success rates which are neatly higher than the ones obtained in [30].

In addition, a necessary condition, which must be satisfied by any algorithm for the singularity avoidance, is proposed. Such condition is not specific to the SAS and may be used for the synthesis of alternative strategies. Analogously, some theoretical considerations concerning the selection of the rotation axis are proposed: they can be used as a starting point for further advances.

The paper is organized as follows. Section II proposes a necessary condition that must be satisfied in order to avoid singularities, while the problem formulation is demanded to Section III. In the same section, the SAS structure proposed in [30] is briefly recalled, while Section IV summarized the foundations of the SAS approach and proposes the novel tuning strategy. Section V reports the outcomes of the validation tests executed on a real manipulator and proposes comparisons with the results achieved in [30]. Final conclusions are drawn in Section VI. Eventually, a graphical abstract has been prepared so as to show the SAS at work.

II. Preliminary Considerations

The analysis in the following will consider a standard anthropomorphic manipulator equipped with a spherical wrist. Its structure is shown in Fig. 2. Frames have been assigned according to the modified Denavit–Hartenberg method [31] and the corresponding kinematic parameters are listed in Table I.

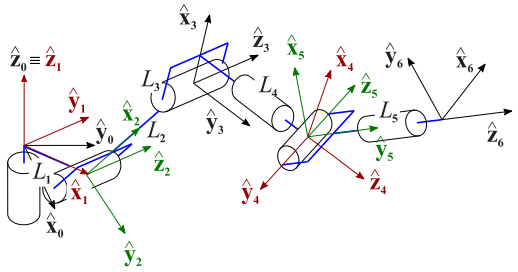

Fig. 2. Manipulator frames assigned according to the modified Denavit–Hartenberg method.

TABLE I

KINEMATIC PARAMETERS OF A TYPICAL ANTHROPOMORPHIC MANIPULATOR

i	α_{i-1}	a_{i-1}	θ_i	d_i
1	0	0	q_1	0
2	$-\pi/2$	L_1	q_2	0
3	0	L_2	q_3	0
4	$-\pi/2$	L_3	q_4	L_4
5	$\pi/2$	0	q_5	0
6	$-\pi/2$	0	q_6	L_5

The SAS is activated, as shown later in this paper, only in proximity of kinematic singularities, i.e., it operates, for a short time, within small regions of the operational space. Inside such regions, trajectories can be reasonably approximated by their tangent and a constant tool-frame orientation can be assumed. Such simplifications allow drawing some considerations concerning the system behavior in the vicinity of singularities and suggest the strategy to be used for their avoidance.

According to the premise, the orientation of the $\hat{\mathbf{z}}_6$ axis is assumed constant in the surroundings of the singularity, while no restrictions are posed on $\hat{\mathbf{x}}_6$ and $\hat{\mathbf{y}}_6$. The following proposition applies.

Proposition 1: Any linear trajectory, executed with constant $\hat{\mathbf{z}}_6$, admits at most one wrist singular configuration if the variable associated with the first joint, i.e., q_1, changes during the motion, or two if q_1 is constant.

Proof: According to the premises, unit vector $\hat{\mathbf{z}}_6 := [z_x \ z_y \ z_z]^T$ is supposed constant. A wrist singularity occurs every time $q_5 = 0$ or, equivalently, when $\hat{\mathbf{z}}_4 = \hat{\mathbf{z}}_6$ (see Fig. 3). Therefore, the first part of the proposition is verified if condition $\hat{\mathbf{z}}_4 = \hat{\mathbf{z}}_6$ applies for a single point of the trajectory.

Proper expressions for $\hat{\mathbf{z}}_4$ can be obtained by solving a direct kinematic problem. Given the parameters of Table I, it is possible to write

$$\hat{\mathbf{z}}_4 = \begin{bmatrix} c_1 \ c_{23} \\ s_1 \ c_{23} \\ s_{23} \end{bmatrix} \tag{1}$$

where $c_1 = \cos(q_1)$, $s_1 = \sin(q_1)$, $c_{23} = \cos(q_2 + q_3)$, and $s_{23} = \sin(q_2 + q_3)$. Let us assume that the trajectory admits a singularity for the following configuration: $q_1 = \bar{\theta}_1$, $q_2 = \bar{\theta}_2$, $q_3 = \bar{\theta}_3$. Evidently, axes 4 and 6 are aligned and the following

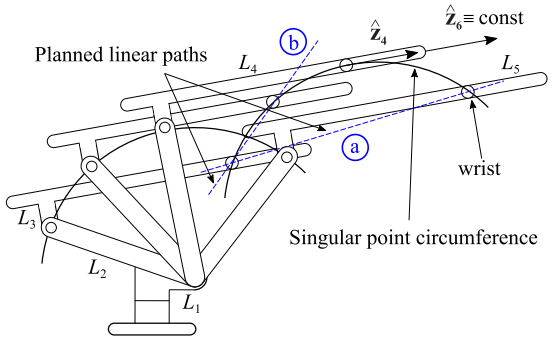

Fig. 3. Side view of the anthropomorphic manipulator. Any constant vector $\hat{\mathbf{z}}_6$ generates a circumference of singular points lying on plane $q_1 = \hat{\theta}_1$. Any straight trajectory can intersect such circumference, at most, into two points.

condition is satisfied:

$$\hat{\mathbf{z}}_4 = \begin{bmatrix} \bar{c}_1 \bar{c}_{23} \\ \bar{s}_1 \bar{c}_{23} \\ \bar{s}_{23} \end{bmatrix} = \begin{bmatrix} z_x \\ z_y \\ z_z \end{bmatrix} = \hat{\mathbf{z}}_6 \tag{2}$$

where $\bar{c}_1 = \cos(\bar{\theta}_1)$, $\bar{s}_1 = \sin(\bar{\theta}_1)$, $\bar{c}_{23} = \cos(\bar{\theta}_2 + \bar{\theta}_3)$, and $\bar{s}_{23} = \sin(\bar{\theta}_2 + \bar{\theta}_3)$. Is it possible to have another singular configuration $q_1 = \bar{\bar{\theta}}_1$, $q_2 = \bar{\bar{\theta}}_2$, and $q_3 = \bar{\bar{\theta}}_3$ along the same trajectory? If yes, the following equation must apply:

$$\begin{bmatrix} \bar{c}_1 \bar{c}_{23} \\ \bar{s}_1 \bar{c}_{23} \\ \bar{s}_{23} \end{bmatrix} = \begin{bmatrix} \bar{\bar{c}}_1 \bar{\bar{c}}_{23} \\ \bar{\bar{s}}_1 \bar{\bar{c}}_{23} \\ \bar{\bar{s}}_{23} \end{bmatrix} = \begin{bmatrix} z_x \\ z_y \\ z_z \end{bmatrix} \tag{3}$$

where $\bar{\bar{c}}_1 = \cos(\bar{\bar{\theta}}_1)$, $\bar{\bar{s}}_1 = \sin(\bar{\bar{\theta}}_1)$, $\bar{\bar{c}}_{23} = \cos(\bar{\bar{\theta}}_2 + \bar{\bar{\theta}}_3)$, and $\bar{\bar{s}}_{23} = \sin(\bar{\bar{\theta}}_2 + \bar{\bar{\theta}}_3)$. If q_1 is variable along the trajectory then, clearly, $\bar{\bar{\theta}}_1 \neq \bar{\theta}_1$, so that (3) cannot be satisfied by any combination of $\bar{\bar{\theta}}_2$ and $\bar{\bar{\theta}}_3$: the trajectory admits only one singularity. Conversely, if q_1 is constant, i.e., $\bar{\bar{\theta}}_1 = \bar{\theta}_1$, then condition $\hat{\mathbf{z}}_4 = \hat{\mathbf{z}}_6$ is satisfied if the following equality applies:

$$\bar{\theta}_2 + \bar{\theta}_3 = \bar{\bar{\theta}}_2 + \bar{\bar{\theta}}_3. \tag{4}$$

Let us study such eventuality. The origin of the fourth frame, i.e., the wrist position, can be obtained from the direct kinematics of the manipulator and written as follows:

$$\mathbf{p}_4 = \begin{bmatrix} (L_3 \ c_{23} - L_4 \ s_{23} + L_2 \ c_2 + L_1)c_1 \\ (L_3 \ c_{23} - L_4 \ s_{23} + L_2 \ c_2 + L_1)s_1 \\ -L_4 \ c_{23} - L_3 \ s_{23} - L_2 \ s_2 \end{bmatrix}. \tag{5}$$

If $\bar{\bar{\theta}}_1 = \bar{\theta}_1$ and (4) apply, then the position of a further singular point $\bar{\mathbf{p}}_4$ can be expressed as follows:

$$\bar{\mathbf{p}}_4 = \begin{bmatrix} (L_3\bar{\bar{c}}_{23} - L_4\bar{\bar{s}}_{23} + L_2\bar{\bar{c}}_2 + L_1)\bar{\bar{c}}_1 \\ (L_3\bar{\bar{c}}_{23} - L_4\bar{\bar{s}}_{23} + L_2\bar{\bar{c}}_2 + L_1)\bar{\bar{s}}_1 \\ -L_4\bar{\bar{c}}_{23} - L_3\bar{\bar{s}}_{23} - L_2\bar{\bar{s}}_2 \end{bmatrix} \tag{6}$$

$$= \begin{bmatrix} (L_3\bar{c}_{23} - L_4\bar{s}_{23} + L_2\bar{\bar{c}}_2 + L_1)\bar{c}_1 \\ (L_3\bar{c}_{23} - L_4\bar{s}_{23} + L_2\bar{\bar{c}}_2 + L_1)\bar{s}_1 \\ -L_4\bar{c}_{23} - L_3\bar{s}_{23} - L_2\bar{\bar{s}}_2 \end{bmatrix} \tag{7}$$

or, equivalently, as follows:

$$\bar{\mathbf{p}}_4 = \begin{bmatrix} k_1 + k_2\bar{\bar{c}}_2 \\ k_3 + k_4\bar{\bar{c}}_2 \\ k_5 + k_6\bar{\bar{s}}_2 \end{bmatrix} \tag{8}$$

where $k_1 := (L_3\bar{c}_{23} - L_4\bar{s}_{23} + L_1)\bar{c}_1$, $k_2 := L_2\bar{c}_1$, $k_3 := (L_3\bar{c}_{23} - L_4\bar{s}_{23} + L_1)\bar{s}_1$, $k_4 := L_2\bar{s}_1$, $k_5 := -L_4\bar{c}_{23} - L_3\bar{s}_{23}$, and $k_6 := -L_2$ are constants. With a few algebraic manipulations, it can be shown that (8) is the equation of a circumference lying on plane $q_1 = \bar{\theta}_1 = \bar{\bar{\theta}}_1$, centered in $[k_1\ k_3\ k_5]^T$, and whose radius is L_2. It contains all the singular points that satisfy $\bar{\theta}_1 = \bar{\bar{\theta}}_1$ and (4). Fig. 3, which shows a schematic side view of the manipulator, provides a graphical interpretation of the result. If the manipulator is executing a linear trajectory, the singular point circumference can be intersected, at most, into two points. ■

Proposition 1 asserts that linear trajectories executed with a constant $\hat{\mathbf{z}}_6$ normally admit no more than one kinematic singularity, since two may only appear for motions in which q_1 is constant. Consequently, if a singularity is avoided with a method which brings back the system to the original trajectory, no further problems have to be expected. Evidently, the singularity avoidance transient may be critical since, according to the premises, the tool-frame orientation is certainly changed, thus invalidating one of the conditions required by Proposition 1: a novel singular point may potentially appear during the transient. Next proposition poses a necessary condition that must be satisfied in the vicinity of the singularity: if it does not apply the system is driven toward a further singularity.

Proposition 2: A necessary condition required for the avoidance of kinematic singularities is that $\text{sgn}(\dot{q}_4)$ and $\text{sgn}(\dot{q}_6)$ do not change during the motion.

Proof: The tool frame associated with the modified trajectory will be indicated in the following by $\widetilde{T}$ in order to distinguish it from T, i.e., from the one associated with the nominal trajectory. The Jacobian matrix for $\widetilde{T}$ is defined as follows:

$$\mathbf{J}_{\widetilde{T}}(\mathbf{q}) := \begin{bmatrix} \mathbf{J}_{v_{\widetilde{T}}}(\mathbf{q}) \\ \hline \mathbf{J}_{\omega_{\widetilde{T}}}(\mathbf{q}) \end{bmatrix}.$$

It is consequently possible to express $\boldsymbol{\omega}_{\widetilde{T}}$, i.e., the angular speed of $\widetilde{T}$, through the following equation:

$$\boldsymbol{\omega}_{\widetilde{T}} = \mathbf{J}_{\omega_{\widetilde{T}}}(\mathbf{q})\,\dot{\mathbf{q}} := \left[\mathbf{J}_{\omega_{\widetilde{T}_1}}(\mathbf{q}) \,|\, \mathbf{J}_{\omega_{\widetilde{T}_2}}(\mathbf{q})\right]\dot{\mathbf{q}} \tag{9}$$

where $\mathbf{J}_{\omega_{\widetilde{T}_1}}(\mathbf{q})$ and $\mathbf{J}_{\omega_{\widetilde{T}_2}}(\mathbf{q})$ are 3×3 matrices obtained by partitioning $\mathbf{J}_{\omega_{\widetilde{T}}}(\mathbf{q})$. $\boldsymbol{\omega}_{\widetilde{T}}$ can also be obtained through the composition rule used for angular velocities. Consequently, it is possible to write

$$\boldsymbol{\omega}_{\widetilde{T}} = \boldsymbol{\omega}_T + {}^0_T\mathbf{R}(\mathbf{q})\,{}^T\boldsymbol{\omega}_{\widetilde{T},T} \tag{10}$$

where $\boldsymbol{\omega}_T$ is the nominal angular speed of the tool frame, while ${}^T\boldsymbol{\omega}_{\widetilde{T},T}$ is the relative angular speed between the nominal tool frame and the modified one, described w.r.t. T. By combining (9) with (10) and by performing some algebraic manipulations, the following equation can be obtained:

$${}^T_0\mathbf{R}(\mathbf{q})\,\mathbf{J}_{\omega_{\widetilde{T}_2}}(\mathbf{q})\,\dot{\tilde{\mathbf{q}}} = {}^T_0\mathbf{R}(\mathbf{q})\,\left[\boldsymbol{\omega}_T - \mathbf{J}_{\omega_{\widetilde{T}_1}}(\mathbf{q})\,\dot{\bar{\mathbf{q}}}\right] + {}^T\boldsymbol{\omega}_{\widetilde{T},T} \tag{11}$$

where $\dot{\bar{\mathbf{q}}} := [\dot{q}_1\,\dot{q}_2\,\dot{q}_3]^T$ while $\dot{\tilde{\mathbf{q}}} := [\dot{q}_4\,\dot{q}_5\,\dot{q}_6]^T$. Practically, $\dot{\bar{\mathbf{q}}}$ and $\dot{\tilde{\mathbf{q}}}$ are partitions of $\dot{\mathbf{q}} := [\dot{\bar{\mathbf{q}}}^T \,|\, \dot{\tilde{\mathbf{q}}}^T]^T$. By defining

$$\hat{\boldsymbol{\omega}} := {}^T_0\mathbf{R}(\mathbf{q})\,\left[\boldsymbol{\omega}_T - \mathbf{J}_{\omega_{\widetilde{T}_1}}(\mathbf{q})\,\dot{\bar{\mathbf{q}}}\right] + {}^T\boldsymbol{\omega}_{\widetilde{T},T}$$

it is finally possible to write (11) as follows:

$${}^T_0\mathbf{R}(\mathbf{q})\,\mathbf{J}_{\omega_{\widetilde{T}_2}}(\mathbf{q})\,\dot{\tilde{\mathbf{q}}} = \hat{\boldsymbol{\omega}} \tag{12}$$

and, in turn, to obtain

$$\dot{\tilde{\mathbf{q}}} = \mathbf{J}^{-1}_{\omega_{\widetilde{T}_2}}(\mathbf{q})\,{}^0_T\mathbf{R}(\mathbf{q})\,\hat{\boldsymbol{\omega}}\,. \tag{13}$$

The structure of (13) can be analyzed by considering the manipulator parameters reported in Table I. To this purpose, let us redefine the joint variables as follows $q_i := \hat{\theta}_i + \theta_i$, where $\hat{\theta}_i$ is the value assumed by the joint variables in the singular point, so that it is constant along the trajectory, while θ_i is the displacement with respect to such value and it clearly changes during the motion. Evidently, $\hat{\theta}_5 = 0$, while no restrictions are imposed on the other $\hat{\theta}_i$s since the discussion in the following applies to any wrist singularity of the workspace.

According to the premises $\hat{\mathbf{z}}_T \equiv \hat{\mathbf{z}}_6$ is constant along the nominal trajectory, so that the tool frame can only rotate around such axis. As a consequence, ${}^0_T\mathbf{R}(\mathbf{q})$ can be obtained from the orientation assumed in the singular point by admitting further rotations around the $\hat{\mathbf{z}}_6$ axis. Practically, the orientation of the tool frame along the nominal trajectory can be obtained by assuming $\mathbf{q} := \left[\hat{\theta}_1\ \hat{\theta}_2\ \hat{\theta}_3\ (\hat{\theta}_4 + \theta_4)\ 0\ (\hat{\theta}_6 + \theta_6)\right]^T$. A few algebraic manipulations make it possible to express the three components of (13) as follows:

$$\dot{q}_4 = \dot{\theta}_4 = \frac{\mathbf{f}_1(\mathbf{q}, \dot{\mathbf{q}}, {}^T\boldsymbol{\omega}_{\widetilde{T},T})}{\sin(\theta_5)} \tag{14}$$

$$\dot{q}_5 = \dot{\theta}_5 = \mathbf{f}_2(\mathbf{q}, \dot{\mathbf{q}}, {}^T\boldsymbol{\omega}_{\widetilde{T},T}) \tag{15}$$

$$\dot{q}_6 = \dot{\theta}_6 = \frac{\mathbf{f}_3(\mathbf{q}, \dot{\mathbf{q}}, {}^T\boldsymbol{\omega}_{\widetilde{T},T})}{\sin(\theta_5)}. \tag{16}$$

Functions $\mathbf{f}_i$, which are not reported for space reasons, are highly nonlinear. However, from (14), it can be inferred that

$$\sin(\theta_5) = \frac{\mathbf{f}_1(\mathbf{q}, \dot{\mathbf{q}}, {}^T\boldsymbol{\omega}_{\widetilde{T},T})}{\dot{\theta}_4}\,. \tag{17}$$

Singularities are certainly avoided if $\theta_5 \neq 0$, i.e., if the sign of θ_5 does not change along a trajectory. Consequently, (17) allows one asserting that such condition can be achieved if during the execution of a trajectory the signs of $\mathbf{f}_1$ and of $\dot{\theta}_4$ always switch simultaneously or, conversely, if they do not switch at all. The first condition can be hardly obtained with any real-time method because of the complexity of the functions involved, so that the second method is the only one that can be actually exploited. Similar considerations apply for $\dot{\theta}_6$. ■

A more accurate formulation of the proposition should state "An almost necessary condition..." since the demonstration shows that an alternative one could be potentially proposed. However, the sign maintenance is the easiest one to be guaranteed. Practically, Proposition 2 asserts that, during any transient for the singularity avoidance, motion directions of joints 4 and 6 must not invert. SAS trajectories fulfill such condition.

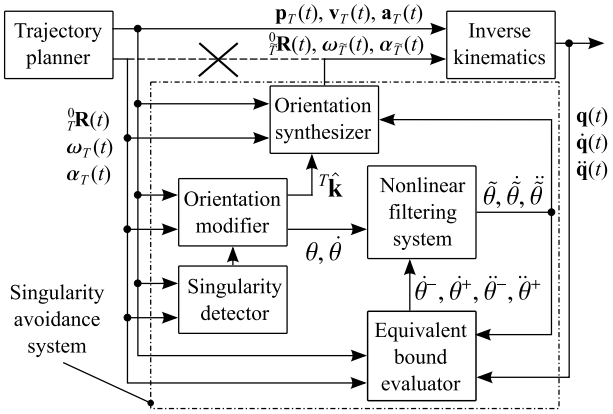

Fig. 4. Schematic of the SAS. The dashed line indicates the orientation reference signals which are normally directly sent to the inverse kinematics. With the proposed approach, such direct connection is eliminated and orientations are processed by the SAS (see the dashed-dotted box).

III. Problem Formulation and SAS Structure

Differently from other methods in the literature, the SAS handles separately the inverse kinematics and the singularity problems. More precisely, the first one is solved through a standard algorithm based on efficient closed-form equations, while singularities are handled by the SAS, which only acts on the tool-frame orientation: as shown in Fig. 4, position references are directly sent to the inverse kinematics block, so as to guarantee that assigned Cartesian paths and time law are preserved with certainty.

The main assumption made in this work is that trajectories are planned and then immediately processed by the SAS in real time, so that there is no dead-time between the planning phase and the trajectory execution. Every time a new trajectory is generated, the following information is provided to the SAS: the path equation, given by $\mathbf{p}_T(s)$ and ${}^0_T\mathbf{R}(s)$, where s is the curvilinear coordinate along the path, and subsequently, at each sample time, the instantaneous values of ${}^0_T\mathbf{R}(t)$, $\mathbf{p}_T(t)$, $\boldsymbol{\omega}_T(t)$, $\mathbf{v}_T(t)$, $\boldsymbol{\alpha}_T(t)$, and $\mathbf{a}_T(t)$. The output of the system is represented by a modified trajectory which fulfills, for all the joints, the following velocity and acceleration constraints:

$$\dot{\mathbf{q}}^- \leq \dot{\mathbf{q}} \leq \dot{\mathbf{q}}^+ \tag{18}$$

$$\ddot{\mathbf{q}}^- \leq \ddot{\mathbf{q}} \leq \ddot{\mathbf{q}}^+ \tag{19}$$

where $\dot{\mathbf{q}}$ and $\ddot{\mathbf{q}}$ are the first and the second time derivatives of joint variables $\mathbf{q} := [q_1, q_2, q_3, q_4, q_5, q_6]^T \in \mathbb{R}^6$, while $\dot{\mathbf{q}}^-, \ddot{\mathbf{q}}^- \in (\mathbb{R}^-)^6$, and $\dot{\mathbf{q}}^+, \ddot{\mathbf{q}}^+ \in (\mathbb{R}^+)^6$ are user-defined bounds for joint velocities and accelerations. Such bounds may also be variable, so as to account, for example, for the presence of torque constraints (see also the discussion in [28]). Far from singularities, trajectories must coincide with the original ones, while in critical configurations, minor orientation displacements can be admitted in order to fulfill (18) and (19). The imposition of specific bounds represent an improvement with respect to classical methods, which generically limit joint velocities and accelerations, but do not explicitly bound them.

The SAS is based on the functional scheme shown in Fig. 4. When the singularity detector block ascertains that the tool frame is moving toward a singularity, the orientation modifier proposes a candidate angular displacement between T and $\widetilde{T}$—where $\widetilde{T}$ indicates the orientation-modified tool frame—so as to allow its avoidance. The displacement is specified by defining an appropriate rotation axis, described through unit vector ${}^T\hat{\mathbf{k}}$, and an angular offset θ. A proper choice of ${}^T\hat{\mathbf{k}}$ and θ allows the fulfillment of the condition posed by Proposition 2. An analytical method for the evaluation of ${}^T\hat{\mathbf{k}}$ was proposed in [30], so that interested readers can refer to that paper for equations and details.

${}^T\hat{\mathbf{k}}$ is directly sent to the orientation synthesizer, i.e., to the block that generates the modified trajectory. Conversely, θ is processed in order to allow smooth and feasible orientation changes. Indeed, any instantaneous change of θ would cause unfeasible joint speeds and accelerations. The nonlinear filtering system (see [32], [33] for details concerning its implementation) is used to solve possible feasibility issues. Its output signal is given by $\tilde{\theta}$, $\dot{\tilde{\theta}}$, and $\ddot{\tilde{\theta}}$. $\tilde{\theta}$ is the best approximation of θ which satisfies the following limits:

$$\dot{\theta}^- \leq \dot{\tilde{\theta}} \leq \dot{\theta}^+ \tag{20}$$

$$\ddot{\theta}^- \leq \ddot{\tilde{\theta}} \leq \ddot{\theta}^+. \tag{21}$$

Bounds $\dot{\theta}^-$, $\dot{\theta}^+$, $\ddot{\theta}^-$, and $\ddot{\theta}^+$, which are computed by the "Equivalent bound evaluator" through the procedure proposed in [30], directly descend from $\dot{\mathbf{q}}^-$, $\ddot{\mathbf{q}}^-$, $\dot{\mathbf{q}}^+$, and $\ddot{\mathbf{q}}^+$, so that (18) and (19) are fulfilled as long as (20) and (21) are satisfied.

IV. Selection of the Rotation Axis and Tuning Procedure

Proper conditions for the singularity avoidance may potentially be devised from (14) and (16). However, functions $\mathbf{f}_1$ and $\mathbf{f}_3$ depend on the Cartesian path through a set of highly nonlinear relationships, so that it was not possible to devise analytical relations for the preservation of the feasibility. For such reason, the SAS is founded on a heuristic strategy proposed in [30], which rationale is explained in the following by means of a simple example based on the two-link planar manipulator shown in Fig. 5.

The ellipsoid of manipulability [34], evaluated in the neighborhood of a singularity, provides some useful information concerning the relationships between velocities in the operational and in the configuration space. In particular, its shape immediately indicates the motion direction which has a minimal impact on the joint speeds and which other should be avoided due to the high velocities it would require. As known, the first one coincides with the major principal axis of the ellipsoid, while the second one with the minor principal axis [34].

Fig. 5a schematically shows what happens when a straight trajectory passes in the surroundings of a kinematic singularity. At the point of minimum distance between trajectory and singularity, the motion of the first joint is subject to a sharp acceleration, with speeds that may be unfeasible. Unit vector ${}^T\hat{\mathbf{k}}$, associated with the major principal axis of the ellipsoid, if evaluated in such point, indicates the motion direction which would produce the lowest joint velocities. ${}^T\hat{\mathbf{k}}$ can be used to generate a small speed $\alpha\,{}^T\hat{\mathbf{k}}$ to be added

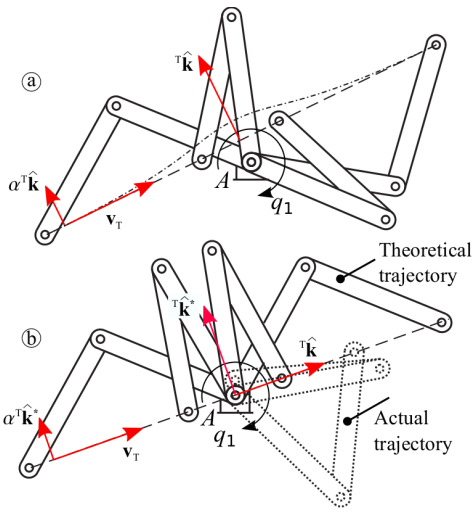

Fig. 5. Case (a): the trajectory (dashed line) passes close to the singularity. The ellipsoid of manipulability indicates ${}^T\hat{\mathbf{k}}$ as a possible escape direction. Velocity $\alpha\,{}^T\hat{\mathbf{k}}$ is added to $\mathbf{v}_T$ in order to modify the path (dashed-dotted line), thus reducing the joint speed. Case (b): the trajectory crosses the singularity. Theoretically, no link flip is required, but minor rounding problems always force it. As a consequence, ${}^T\hat{\mathbf{k}}^*$ must be used instead of ${}^T\hat{\mathbf{k}}$, which is suggested by the ellipsoid of manipulability, in order to escape from the singularity.

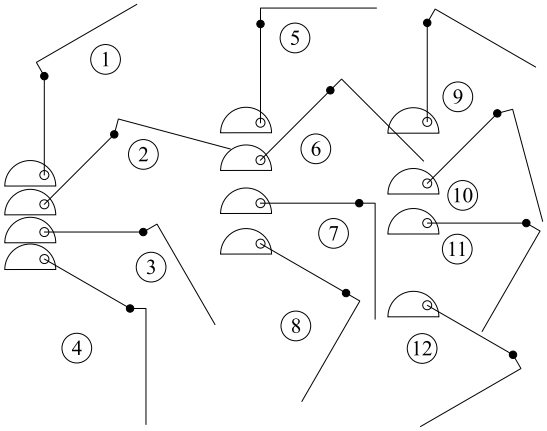

Fig. 6. Schematic of the 12 poses assumed by links 2 and 3 for the experimental validation of the SAS.

to $\mathbf{v}_T$, so as to generate a path passing farther from the singularity. Consequently, the speed of the first joint will be lowered.

Trajectories crossing singular points must be handled differently. Such trajectories, as suggested by the alignment between the major principal axis of the ellipsoid and the given path, may be theoretically executed by avoiding the π turn of the first joint (see also Fig. 5(b). However, under actual operating conditions, any small numerical rounding in the forward/inverse kinematics forces an undesired sudden turn of joint 1. As a consequence, it is always better to force a controlled rotation of joint 1. To this purpose, a speed $\alpha\,{}^T\hat{\mathbf{k}}^*$ can be added to the nominal $\mathbf{v}_T$, where ${}^T\hat{\mathbf{k}}^*$ is obtained by rotating ${}^T\hat{\mathbf{k}}$ of an appropriate angle. In Fig. 5, such angle is equal to $\pi/2$ but, for the problem at hand, the actual amplitude was chosen through the procedure later proposed in this section.

In the planar example just considered, kinematic singularities are avoided by modifying linear velocities and, in turn, the path. However, the same concept also applies for angular velocities, so that, for a 6 degrees-of-freedom manipulator, singular configurations can be avoided by changing the tool-frame orientation instead of its path. To this purpose, the orientation modifier proposes a candidate rotation in the following form:

$$ {}^T\mathbf{k} := \theta\ {}^T\hat{\mathbf{k}}\,. \tag{22}$$

A characteristic of rotation axis ${}^T\hat{\mathbf{k}}$ is that it always lies on the xy plane of the tool frame. The association of a proper value of θ to ${}^T\hat{\mathbf{k}}$ represents a complex problem, since no evident theoretical considerations are available for the synthesis of adequate analytical equations. For evident reasons, small values of θ are desirable. In the same way, the angular deviation from the nominal trajectory should last for a short period: curvilinear coordinates $s_a := s^* - d_a$ and $s_d := s^* + d_a$, at which the SAS must be, respectively, activated and deactivated, are very important. s^* indicates a point along the path which is located just before the singular configuration and d_a is the activation distance which must be kept as small as possible.

θ and d_a have been tuned through a procedure totally based on simulative tests. Its outcomes have been later verified on the actual manipulator. A set of wrist singular points, uniformly distributed in the workspace, were first selected by aligning the fourth and the sixth joint axes, i.e., by posing $q_5 = 0$, and, subsequently, by assigning all possible combinations of q_2 and q_3 taken from the following sets: $q_2 \in \{-\pi/2\ \ -\pi/4\ \ \ 0\ \ \pi/6\}$, $q_3 \in \{-\pi/6\ \ 0\ \ \pi/6\}$. In facts, as shown in Fig. 6, the combinations of q_2 and q_3 were chosen so as to cover the whole workspace. Upper and lower bounds on q_2 and q_3 were imposed by the end-strokes of the actual manipulator.

A "star" of straight trajectories passing through the resulting 12 singular points was then generated so as to cover all possible directions in the 3-D space. Joint variables q_1, q_4, and q_6 have no influence on the singularity analysis: the results obtained apply independently of their values. The tuning set is potentially composed by 4440 unfeasible trajectories (370 for each singular point); however, since some of them partially fall outside the workspace, the actual one contains 3110 cases. The following bounds have been assumed for velocities and accelerations ($i = 1, 2, \ldots, 6$): $\dot{q}_i^- = -10$ rad s^{-1}, $\dot{q}_i^+ = 10$ rad s^{-1}, $\ddot{q}_i^- = -25$ rad s^{-2}, and $\ddot{q}_i^+ = 25$ rad s^{-2}.

The tuning procedure starts by first choosing, for each trajectory of the tuning set, the proper rotation axis ${}^T\hat{\mathbf{k}}$ [30] and, then, the trajectory is executed at the maximum speed (0.4 ms^{-1}) by activating the SAS and by assuming a constant value of θ for the whole segment: the procedure is repeated by progressively increasing θ until a feasible trajectory is obtained. At the end of the process, a threshold value $\overline{\theta}$ is associated with each feasible trajectory of the tuning set.

As early asserted, since tuning trajectories exactly cross singular configurations, ${}^T\hat{\mathbf{k}}$ must be perturbed with respect

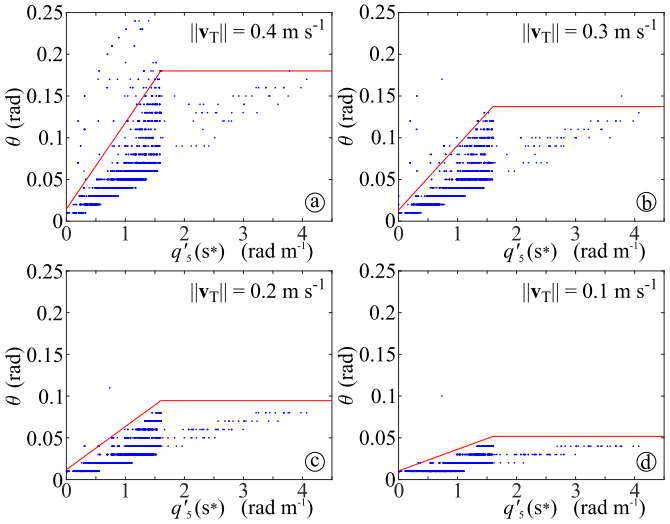

Fig. 7. For each trajectory of the testset, a blue dot associates $q_5'(s^*)$ to the minimum value $\overline{\theta}$ which guarantees feasibility. Red lines represent the output of (24) and are used by the SAS for the evaluation of the tool-frame rotation angle.

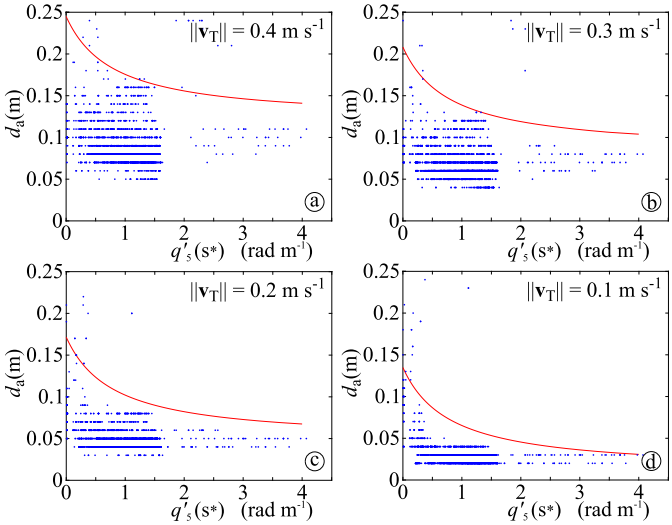

Fig. 8. For each trajectory of the testset, a blue dot associates $q_5'(s^*)$ to the minimum value d_a which guarantees feasibility. Red lines represent the output of (25) and are used for the evaluation of the SAS activation distance.

to the one suggested by the ellipsoid of manipulability: the tuning procedure was repeated for different orientations of ${}^T\hat{\mathbf{k}}$—which must always lie on the xy plane of the tool frame—trying to minimize the average value of all $\overline{\theta}$s: the best performances were achieved by adopting a rotation for ${}^T\hat{\mathbf{k}}$ in the range [0.8, 0.9] rad.

The acquired data highlighted, for each trajectory, a relationship between $\overline{\theta}$ and the derivative of q_5 with respect to s, i.e., $q_5'(s^*) = |[dq_5(s)]/ds|_{s=s^*}$, where s^* indicates a position along the path located just before the singular configuration. Such relationship is shown in Fig. 7(a): for each trajectory, a dot indicates the value of $\overline{\theta}$ associated with the corresponding $q_5'(s^*)$. Such information was used to define the following function:

$$\overline{\theta}\left[q_5'(s^*)\right] := a + b\ \min\left\{\left|q_5'(s^*)\right|, c\right\} \tag{23}$$

which output, obtained by assuming $a = 0.0147$, $b = 0.1033$, and $c = 1.6$ is shown by a red line in Fig. 7(a). Coefficients a and b are the intercept and the slope coefficients of the leftmost linear segment, respectively. $\overline{\theta}$ is superiorly saturated by means of c. For the problem at hand, c was chosen so as to guarantee a maximum angular displacement equal to 0.18 rad (10.31 deg). It is worth mentioning that smaller angular displacements may be imposed by reducing c, but lower travel speeds must be assumed in order to maintain high success rates. With the values chosen for the three coefficients, 91.0% trajectories lie below the red line and, consequently, are feasible.

The angular displacements obtained through (23) are excessive if used for $\|\mathbf{v}_T\|$ lower than 0.4 ms^{-1} and, consequently, $\overline{\theta}$ is subsequently downscaled according to the following equation:

$$\theta := \overline{\theta}_0 + \frac{\overline{\theta} - \overline{\theta}_0}{0.4}\|\mathbf{v}_T\|\ . \tag{24}$$

The red lines in Fig. 7 show the output of (24) at different speeds for $\overline{\theta}_0 = 0.009$. $\overline{\theta}_0$ is not critical; it represents the minimum angular displacement to be introduced when the SAS is activated. It can be noticed that the percentage of points above the red lines, corresponding to unfeasible trajectories, decreases together with the speed. For $\|\mathbf{v}_T\| = 0.1$ ms^{-1}, the success rate increases up to 96.8%. Evidently, $\|\mathbf{v}_T\| = 0.4$ ms^{-1} is a critical speed which strongly solicits some joints and which would potentially require higher values for θ.

The time interval during which the SAS modifies the nominal trajectory depends on d_a and must be kept as small as possible. To this purpose, the tuning set was newly executed by evaluating θ according to (24) and by progressively reducing d_a until feasibility was lost. Simulations pointed out a relationship between $q_5'(s^*)$ and d_a: the higher $\left|q_5'(s^*)\right|$, the lower d_a. In the same way, a relationship between d_a and $\|\mathbf{v}_T\|$ was observed. Good success results were obtained by selecting d_a through the following hyperbolic function $(d_a - \overline{d})\left(\left|q_5'(s^*)\right| - \overline{q}\right) = k$ or, equivalently

$$d_a := \frac{\overline{d}\left|q_5'(s^*)\right| + k - \overline{q}\,\overline{d}}{\left|q_5'(s^*)\right| - \overline{q}} \tag{25}$$

with

$$\overline{d} := d_0 + \frac{d_1}{0.4}\|\mathbf{v}_T\| \tag{26}$$

and where $k = 0.1$, $d_0 = -0.027$, $d_1 = 0.147$, and $\overline{q} = -0.8$. The output of (25) is represented by the red lines shown in Fig. 8. Coefficients k, $\overline{d}$, and $\overline{q}$ were tuned so as to bound as many samples as possible below the red line of Fig. 8(a), i.e., the one corresponding to the maximum speed: k acts on the shape of the hyperbole, while $\overline{d}$ and $\overline{q}$ change its vertical and horizontal displacement, respectively. Then, the obtained value of $\overline{d}$ is subsequently scaled down by means of (26), so as to account for smaller longitudinal speeds: obviously $d_0 + d_1$ must coincide with the value of $\overline{d}$ previously obtained.

TABLE II

COMPARISON BETWEEN THE SUCCESS RATES OBTAINED THROUGH THE OLD TUNING PROCEDURE (OTP) PROPOSED IN [30] AND THE NEW TUNING PROCEDURE (NTP) PROPOSED IN THIS PAPER. d INDICATES THE DISTANCE BETWEEN TRAJECTORIES AND SINGULAR POINTS

		$\|\mathbf{v}_T\|$ (m s^{-1})			
d (m)		0.1	0.2	0.3	0.4
$0 \cdot 10^{-3}$	OTP	96.2%	90.3%	84.5%	76.2%
	NTP	97.7%	96.8%	95.1%	92.3%
$1 \cdot 10^{-3}$	OTP	72.7%	68.4%	66.0%	63.1%
	NTP	91.1%	87.8%	85.4%	82.7%
$2 \cdot 10^{-3}$	OTP	68.8%	66.5%	58.7%	53.1%
	NTP	94.2%	91.0%	88.2%	85.9%
$5 \cdot 10^{-3}$	OTP	69.7%	65.3%	53.3%	48.4%
	NTP	96.2%	94.7%	92.7%	90.7%
$10 \cdot 10^{-3}$	OTP	70.9%	63.2%	53.8%	43.8%
	NTP	96.8%	95.3%	94.0%	91.9%

The subdivision between d_0 and d_1 is made by maximizing, for all possible speeds, the number of samples lying below the red lines.

The tuning procedure only accounts for trajectories passing through singularities. In order to verify if the obtained parameters can be adopted to manage trajectories which do not exactly cross singularities, they were tested by also considering alternative scenarios. In particular, for each one of the 12 test configurations, 4 additional points were placed 10^{-3} m far from the singularity and, in each of them, a "star" of 370 trajectories was generated. The experiment was then repeated by considering 4 more points located $2 \cdot 10^{-3}$ m far from the singularity, and so on. The obtained success rates are listed in Table II, where they are compared with the results achieved through the tuning procedure proposed in [30]. The tuning procedure, which is very fast and easily adaptable to alternative manipulators or working conditions, always guarantees higher success rates with respect to [30]. Evidently, the best performances are achieved for trajectories crossing singularities, since they were used for the system tuning. However, for primitives passing close to singular points, the success rate drop is limited and, in any case, it is smaller than the one resulting with the approach proposed in [30]. The difference is particularly evident for high values of $\|\mathbf{v}_T\|$.

It must be pointed out that 100% success rate can never be reached for several reasons. Many configurations in Fig. 6 (see for example 4, 7, 8, 11, and 12) admit trajectories passing close or through shoulder singularities, which are not managed by the SAS. Furthermore, some trajectories are almost singular everywhere and, finally, some others are characterized by two singular configurations.

V. EXPERIMENTAL RESULTS

The SAS has been tested by means of a Comau Smart SiX 6-1.4 anthropomorphic manipulator. An external Linux-RTAI PC is used to generate the trajectories and to process them with the SAS at a sample rate equal to $2 \cdot 10^{-3}$ s. The obtained reference signals are sent, with the same sample rate, to the feedback control loops of the robot controller through a real-time Ethernet connection.

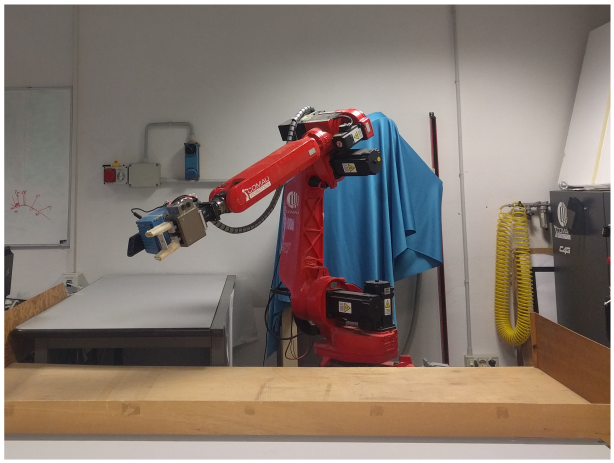

Fig. 9. Presence of desks limits the workspace of the Comau manipulator used for the experiments.

TABLE III

SUCCESS RATES OBTAINED WITH THE ACTUAL MANIPULATOR. d INDICATES THE DISTANCE BETWEEN TRAJECTORY AND SINGULAR POINT

	$\|\mathbf{v}_T\|$ (m s^{-1})			
d (m)	0.1	0.2	0.3	0.4
0	96.6%	94.9%	94.7%	93.2%
$1 \cdot 10^{-3}$	95.1%	93.9%	92.9%	91.1%
$2 \cdot 10^{-3}$	96.3%	95.0%	93.9%	92.5%
$5 \cdot 10^{-3}$	97.3%	96.5%	95.4%	94.2%
$10 \cdot 10^{-3}$	97.9%	97.0%	96.5%	95.2%

As shown in Fig. 9, the manipulator workspace is limited by the presence of desks. As a consequence, only a part of the simulated tests were replicated in the real environment and, more precisely, the ones corresponding to configurations 1, 2, 5, and 9 shown in Fig. 6. The experimentally acquired success rates were even better than simulated ones, as proved by Table III. The reason of such performances is that unmanageable configurations occur more frequently in areas which are precluded to the real manipulator.

Fig. 10 shows a typical transient for joints 4 and 6, i.e., the most solicited ones. The figure proves that, differently from other approaches in the literature, the proposed strategy does not simply reduce joint velocities and accelerations, but it explicitly bounds them between the given limits. Similar results were obtained for all the trajectories of the test set. Another detail, still pointed out by Fig. 10, concerns the exchange of position between joints 4 and 6: it occurs for all the trajectories and it is a direct consequence of Proposition 2. In order to prove such assertion, let us consider a simplified representation of (14) and (16) obtained for very common operating conditions. Many applications do not require the tool-frame rotation, i.e., $\hat{\mathbf{x}}_6$ and $\hat{\mathbf{y}}_6$ can be assumed constant together with $\hat{\mathbf{z}}_6$, so that $\boldsymbol{\omega}_T = \mathbf{0}$. Furthermore, the SAS strategy actuates the angular displacement between nominal and modified tool frame when the system is sufficiently far

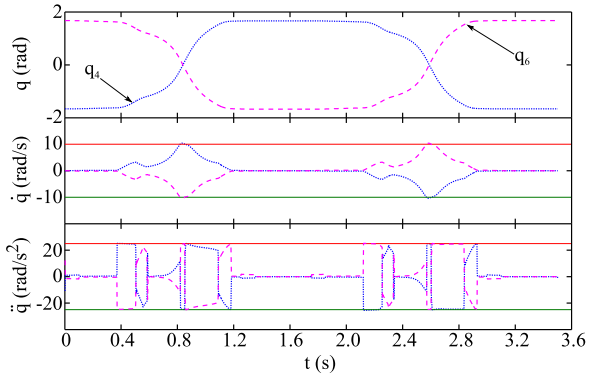

Fig. 10. Velocity and acceleration signals for joints 4 and 6 associated with two horizontal trajectories passing through a singular configuration: the given bounds are fulfilled.

from the singularity: close to critical configurations, it can be reasonably assumed ${}^T\boldsymbol{\omega}_{\tilde{T},T} = \mathbf{0}$ and, additionally, $\sin(\theta_5) \simeq \theta_5$ and $\cos(\theta_5) \simeq 1$. Bearing in mind such premises, (14) and (16) simplify as follows:

$$\dot{\theta}_4 = \dot{\theta}_1 \mathrm{c}_{23} + \frac{\dot{\theta}_1 \mathrm{c}_4 \mathrm{s}_{23} + (\dot{\theta}_2 + \dot{\theta}_3)\mathrm{s}_4}{\theta_5} \tag{27}$$

$$\dot{\theta}_6 = -\frac{\dot{\theta}_1 \mathrm{c}_4 \mathrm{s}_{23} + (\dot{\theta}_2 + \dot{\theta}_3)\mathrm{s}_4}{\theta_5} \tag{28}$$

where $\mathrm{c}_4 = \cos(\hat{\theta}_4 + \theta_4) = \cos(q_4)$, $\mathrm{s}_4 = \sin(\hat{\theta}_4 + \theta_4) = \sin(q_4)$, $\mathrm{c}_{23} = \cos(\hat{\theta}_2 + \hat{\theta}_3 + \theta_2 + \theta_3) = \cos(q_2 + q_3)$, and $\mathrm{s}_{23} = \sin(\hat{\theta}_2 + \hat{\theta}_3 + \theta_2 + \theta_3) = \sin(q_2 + q_3)$. Close to the singularity $\theta_5 \simeq 0$, so that from (27) and (28), it is possible to infer that

$$\dot{\theta}_4 \simeq \frac{\dot{\theta}_1 \mathrm{c}_4 \mathrm{s}_{23} + (\dot{\theta}_2 + \dot{\theta}_3)\mathrm{s}_4}{\theta_5} = -\dot{\theta}_6 \tag{29}$$

i.e., the velocities of joints 4 and 6 are each other opposite so that the positions of the corresponding joints swap. It is important to stress that the simplifications were only introduced in order to propose a compact representation of (14) and (16), but (29) is still valid even when they do not apply.

The novel SAS performances can also be appreciated by means of the proposed multimedia attachment. The velocity assumed is always equal to $\|\mathbf{v}_T\| = 0.4$ ms^{-1}. Experiment 1 shows the execution of random trajectories lying on a vertical plane. For time reasons, the video shows the first seven trajectories of the 100 that were actually executed. Experiment 2 shows some of the trajectories of the test set. They are relative to configurations 1, 2, and 5 shown in Fig.6. Some of them are particularly critical since they are close to a workspace border or to an elbow singularity. All the trajectories that were classified "manageable" by the algorithm were actually executed with the aid of the SAS and feasibility was never lost, i.e., all trajectories were feasible with respect to the imposed velocity and acceleration constraints.

For which concerns the performances, the average computational time, obtained with an Intel Core2 Duo PC running at 3.0GHz, was equal to $4.211 \cdot 10^{-5}$ s. It typically spans in the range $[2.800 \cdot 10^{-5}, 1.690 \cdot 10^{-4}]$ s: evaluation times are, roughly, four times smaller than the ones obtained in [28] and are plenty compatible with the manipulator sample time ($2 \cdot 10^{-3}$ s).

VI. Conclusion

The technique proposed in this paper for the automatic handling of wrist singularities occurring in nonredundant anthropomorphic manipulators is explicitly suited to trajectories planned on-the-fly, being totally based on a real-time strategy. Differently from alternative methods in the literature, it preserves the user-defined Cartesian path and time law. In addition, joint velocities and accelerations are not generically reduced, but they are explicitly limited within assigned bounds. The tuning procedure proposed in this work enhances the performances achieved in an early work, by allowing higher success rates. Results were experimentally validated on a real manipulator by means of extensive tests. A very good agreement has been verified between simulated and experimental results.

At the moment, some preliminary tests have been performed by considering curvilinear paths and by assuming the algorithm "as it is." Clearly, Proposition 1 does no more apply, so that multiple singular points may appear along a single path. The success rate necessarily decreases depending on the path curvature and on the orientation of the osculating circle associated with the path, but preliminary statistics show very promising performances.

References

[1] A. Liégeois, "Automatic supervisory control of the configuration and behavior of multibody mechanisms," *IEEE Trans. Syst., Man, Cybern.*, vol. SMC-7, no. 12, pp. 868–871, Dec. 1977.

[2] J. Baillieul, J. Hollerbach, and R. Brockett, "Programming and control of kinematically redundant manipulators," in *Proc. 23rd IEEE Conf. Decis. Control*, Las Vegas, NV, USA, Dec. 1984, pp. 768–774.

[3] A. Maciejewski and C. A. Klein, "Obstacle avoidance for kinematically redundant manipulators in dynamically varying environments," *Int. J. Robot. Res.*, vol. 4, no. 3, pp. 109–117, Sep. 1985.

[4] Y. Nakamura, H. Hanafusa, and T. Yoshikawa, "Task-priority based redundancy control of robot manipulators," *Int. J. Robot. Res.*, vol. 6, no. 2, pp. 3–15, Jun. 1987.

[5] S. Chiaverini, "Singularity-robust task-priority redundancy resolution for real-time kinematic control of robot manipulators," *IEEE Trans. Robot. Autom.*, vol. 13, no. 3, pp. 398–410, Jun. 1997.

[6] Y. Nakamura and H. Hanafusa, "Inverse kinematic solutions with singularity robustness for robot manipulator control," *J. Dyn. Syst., Meas., Control*, vol. 108, no. 3, pp. 163–171, Sep. 1986.

[7] C. W. Wampler, "Manipulator inverse kinematic solutions based on vector formulations and damped least-squares methods," *IEEE Trans. Sys., Man, Cyber.*, vol. SMC-16, no. 1, pp. 93–101, Jan. 1986.

[8] L. Sciavicco and B. Siciliano, "A solution algorithm to the inverse kinematic problem for redundant manipulators," *IEEE J. Robot. Autom.*, vol. RA-4, no. 4, pp. 403–410, Aug. 1988.

[9] P. Chiacchio, S. Chiaverini, L. Sciavicco, and B. Siciliano, "Closed-loop inverse kinematics schemes for constrained redundant manipulators with task space augmentation and task priority strategy," *Int. J. Robot. Res.*, vol. 10, no. 4, pp. 410–425, Aug. 1991.

[10] L. J. Everett, J. C. Colson, and B. W. Mooring, "Automatic singularity avoidance using joint variations in robot task modification," *IEEE Robot. Autom. Mag.*, vol. 1, no. 3, pp. 13–19, Sep. 1994.

[11] S. Chiaverini, B. Siciliano, and O. Egeland, "Review of the damped least-squares inverse kinematics with experiments on an industrial robot manipulator," *IEEE Trans. Control Syst. Technol.*, vol. 2, no. 2, pp. 123–134, Jun. 1994.

[12] C. Qiu, Q. Cao, and S. Miao, "An on-line task modification method for singularity avoidance of robot manipulators," *Robotica*, vol. 27, no. 4, pp. 539–546, Jul. 2009.
[13] W. Xu, J. Zhang, B. Liang, and B. Li, "Singularity analysis and avoidance for robot manipulators with nonspherical wrists," *IEEE Trans. Ind. Electron.*, vol. 63, no. 1, pp. 277–290, Jan. 2016.
[14] A. Bemporad, T.-J. Tarn, and N. Xi, "Predictive path parameterization for constrained robot control," *IEEE Trans. Control Syst. Technol.*, vol. 7, no. 6, pp. 648–656, Nov. 1999.
[15] D. Lam, C. Manzie, and M. C. Good, "Model predictive contouring control for biaxial systems," *IEEE Trans. Control Syst. Technol.*, vol. 21, no. 2, pp. 552–559, Mar. 2013.
[16] A. Hladio, C. Nielsen, and D. Wang, "Path following for a class of mechanical systems," *IEEE Trans. Control Syst. Technol.*, vol. 21, no. 6, pp. 2380–2390, Nov. 2013.
[17] M. Böck and A. Kugi, "Real-time nonlinear model predictive path-following control of a laboratory tower crane," *IEEE Trans. Control Syst. Technol.*, vol. 22, no. 4, pp. 1461–1473, Jul. 2014.
[18] T. Faulwasser, T. Weber, P. Zometa, and R. Findeisen, "Implementation of nonlinear model predictive path-following control for an industrial robot," *IEEE Trans. Control Syst. Technol.*, vol. 25, no. 4, pp. 1505–1511, Jul. 2017.
[19] J. E. Bobrow, S. Dubowsky, and J. S. Gibson, "Time-optimal control of robotic manipulators along specified paths," *Int. J. Robot. Res.*, vol. 4, no. 3, pp. 3–17, Sep. 1985.
[20] C. Guarino Lo Bianco and F. Ghilardelli, "Real-time planner in the operational space for the automatic handling of kinematic constraints," *IEEE Trans. Autom. Sci. Eng.*, vol. 11, no. 3, pp. 730–739, Jul. 2014.
[21] F. Lange and M. Suppa, "Predictive path-accurate scaling of a sensor-based defined trajectory," in *Proc. IEEE Int. Conf. Robot. Autom. (ICRA)*, May 2014, pp. 754–759.
[22] W. Tillmann, E. Vogli, and B. Krebs, "Influence of the spray angle on the characteristics of atmospheric plasma sprayed hard material based coatings," *J. Therm. Spray Technol.*, vol. 17, nos. 5–6, pp. 948–955, Dec. 2008.
[23] P. J. From and J. T. Gravdahl, "A real-time algorithm for determining the optimal paint gun orientation in spray paint applications," *IEEE Trans. Autom. Sci. Eng.*, vol. 7, no. 4, pp. 803–816, Oct. 2010.
[24] P. J. From, J. Gunnar, and J. T. Gravdahl, "Optimal paint gun orientation in spray paint applications–experimental results," *IEEE Trans. Autom. Sci. Eng.*, vol. 8, no. 2, pp. 438–442, Apr. 2011.
[25] G. Schreiber, M. Otter, and G. Hirzinger, "Solving the singularity problem of non-redundant manipulators by constraint optimization," in *Proc. IEEE/RSJ Int. Conf. Intell. Robots Syst.*, vol. 3, Oct. 1999, pp. 1482–1488.
[26] W. Decré, H. Bruyninckx, and J. D. Schutter, "Extending the iTaSC constraint-based robot task specification framework to time-independent trajectories and user-configurable task horizons," in *Proc. IEEE Int. Conf. Robot. Autom.*, May 2013, pp. 1941–1948.
[27] Y. Huang, Y. S. Yong, Y. Chiba, T. Arai, T. Ueyama, and J. Ota, "Kinematic control with singularity avoidance for teaching-playback robot manipulator system," *IEEE Trans. Autom. Sci. Eng.*, vol. 13, no. 2, pp. 729–742, Apr. 2016.
[28] F. Ghilardelli, C. Guarino Lo Bianco, and M. Locatelli, "Smart changes of the end-effector orientation for the automatic handling of singular configurations," *IEEE/ASME Trans. Mechatronics*, vol. 21, no. 4, pp. 2154–2164, Aug. 2016.
[29] M. Raineri, C. Guarino Lo Bianco, M. Locatelli, and S. Perri, "A real-time strategy for the management of kinematic singularities: New progresses," in *Proc. 21st Int. Conf. Models Autom. Robot. (MMAR)*, Miedzyzdroje, Poland, Aug. 2016, pp. 345–350.
[30] C. Guarino Lo Bianco and M. Raineri, "An automatic system for the avoidance of wrist singularities in anthropomorphic manipulators," in *Proc. IEEE Int. Conf. Autom. Sci. Eng. (CASE)*, Aug. 2017, pp. 1302–1309.
[31] J. J. Craig, *Introduction to Robotics Mechanics and Control*, 3rd ed. Upper Saddle River, NJ, USA: Prentice-Hall, 2005.
[32] C. Guarino Lo Bianco and F. M. Wahl, "A novel second order filter for the real-time trajectory scaling," in *Proc. IEEE Int. Conf. Robot. Autom.*, Shanghai, China, May 2011, pp. 5813–5818.
[33] O. Gerelli and C. Guarino Lo Bianco, "A discrete-time filter for the on-line generation of trajectories with bounded velocity, acceleration, and jerk," in *Proc. IEEE Int. Conf. Robot. Autom.*, Anchorage, AK, USA, May 2010, pp. 3989–3994.
[34] L. Sciavicco, B. Siciliano, L. Villani, and G. Oriolo, *Robotics: Modelling, Planning and Control* (Advanced Textbooks in Control adnd Signal Processing). Berlin, Germany: Springer, 2011.